Erythrocyte Membrane-Enveloped Polymeric Nanoparticles as Nanovaccine for Induction of Antitumor Immunity against Melanoma

Yuanyuan Guo,[†,#] Dong Wang,[†,#] Qingle Song,[†] Tingting Wu,[†] Xiangting Zhuang,[†] Yuling Bao,[†] Miao Kong,[†] Yan Qi,[†] Songwei Tan,[†] and Zhiping Zhang*[,†,‡,§]

[†]Tongji School of Pharmacy, [§]Hubei Engineering Research Center for Novel Drug Delivery System, [‡]National Engineering Research Center for Nanomedicine, Huazhong University of Science and Technology, Wuhan, 430030, China. [#]Dong Wang and Yuanyuan Guo contributed equally to this work.

ABSTRACT Cancer immunotherapy is mainly focused on manipulating patient's own immune system to recognize and destroy cancer cells. Vaccine formulations based on nanotechnology have been developed to target delivery antigens to antigen presenting cells (APCs), especially dendritic cells (DCs) for efficiently induction of antigen−specific T cells response. To enhance DC targeting and antigen presenting efficiency, we developed erythrocyte membrane-enveloped poly(D,L-lactide-*co*-glycolide) (PLGA) nanoparticles for antigenic peptide ($hgp100_{25-33}$) and toll-like receptor 4 agonist, monophosphoryl lipid (MPLA). A Mannose-inserted membrane structure was constructed to actively target APCs in the lymphatic organ, and redox-sensitive peptide-conjugated PLGA nanoparticles were fabricated which prone to cleave in the intracellular milieu. The nanovaccine demonstrated the retained protein content in erythrocyte and enhanced *in vitro* cell uptake. An antigen-depot effect was observed in the administration site with promoted retention in draining lymph nodes. Compared with other formulations after intradermal injection, the nanovaccine prolonged tumor-occurring time, inhibited tumor growth, and suppressed tumor metastasis in prophylactic, therapeutic, and metastatic melanoma models, respectively. Additionally, we revealed that nanovaccine effectively enhanced IFN-γ secretion and $CD8^+$ T cell response. Taken together, these results demonstrated the great potential in applying an erythrocyte membrane-enveloped polymeric nanoplatform for an antigen delivery system in cancer immunotherapy.

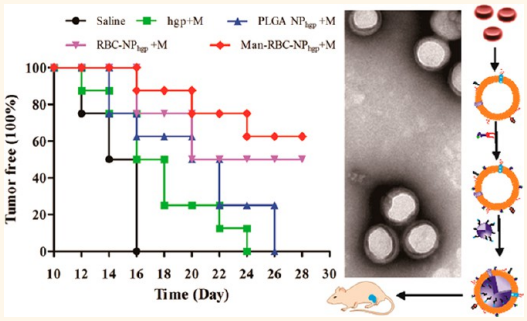

KEYWORDS: cancer vaccine · red blood cell · nanoparticles · dendritic cells · immunotherapy

The current cancer immunotherapies, such as cytokines treatment, immune checkpoint blockade immunotherapy, adoptive immunotherapy, and chimeric antigen receptor T cell immunotherapy (CAR-T), have shown meaningful benefits for cancer therapy.[1] Among them, dendritic cell (DC)-based immunotherapy plays a crucial role in cancer treatment from the unique features of DCs in the immune system. As the most potent professional antigen presenting cells (APCs), DCs are considered as the important initiator of immunity for generation of specific cytotoxic T lymphocyte (CTL)-mediated immunotherapy against tumors. To promote T cell activation, DCs have to migrate to the proximal draining lymph nodes (LNs) after capture of tumor antigens, and subsequently secrete the pro-inflammatory cytokines.[2] Provenge, the first FDA-approved therapeutic cancer vaccine, is based on the *ex vivo* pulsing of autologous DCs with prostatic acid phosphatase, an antigen associated with a subset of prostate cancers.[3] Despite DC-based immunotherapy presenting the induction of antigen-specific responses in preclinical animal models and human clinical studies, the isolation, culture, and antigen-pulsing of DCs are still at a high cost, extremely labor-intensive, and less reproducible. Moreover, transplanted DCs which could home in on the LNs were only 0.5−2.0% and thus not enough to induce efficient T cell responses.[4,5] To avoid the

* Address correspondence to zhipingzhang@mail.hust.edu.cn.

Received for review February 13, 2015 and accepted July 8, 2015.

Published online July 08, 2015
10.1021/acsnano.5b01042

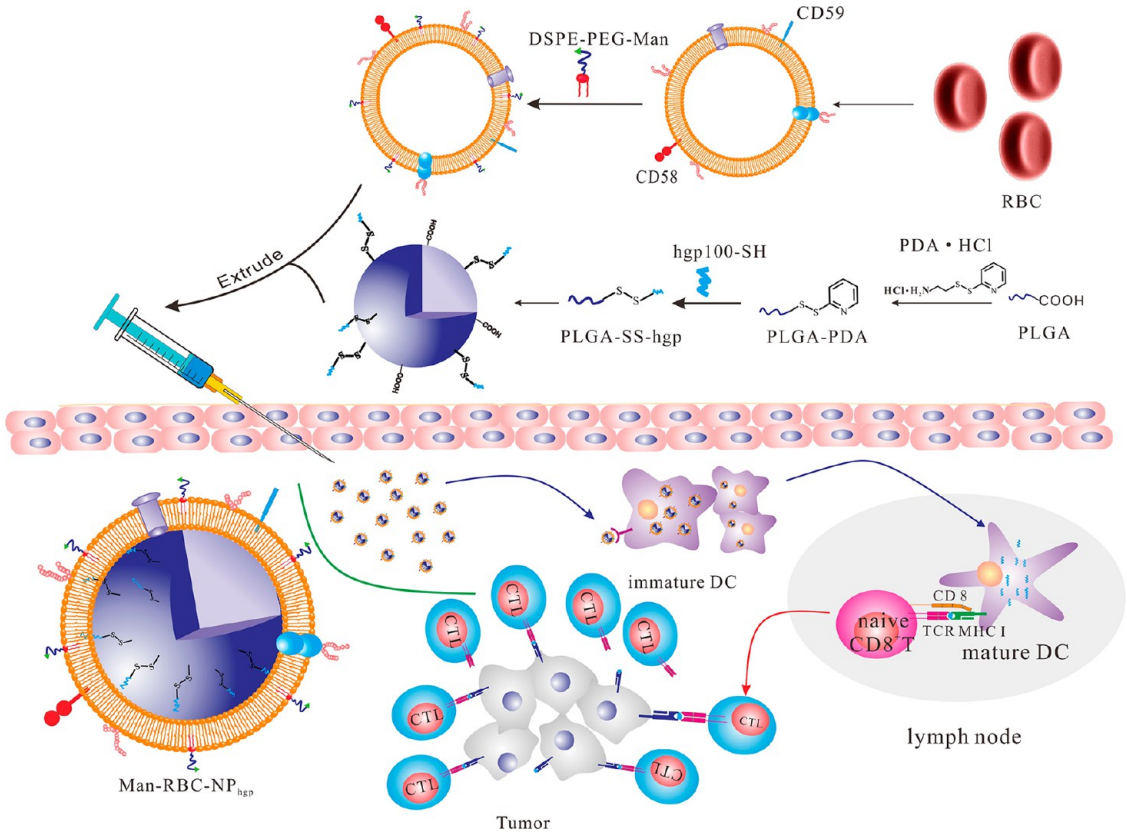

Figure 1. Schematic illustration of the preparation of Man-RBC membrane-coated PLGA-SS-hgp100 nanoparticles (Man-RBC-NP$_{hgp}$) and induction of antitumor immunity.

tedious *ex vivo* DC-based procedure and present a sufficient amount of antigen to DsC for efficient induction of antitumor CTL responses, nanotechnology is applied for sustained and targeted antigen delivery to DCs.[6−8] In this regard, nanoparticles (NPs) of natural or synthetic origin have been developed to enhance the efficacy of therapeutic agents for antigen delivery.[7,9] Soluble antigens are encapsulated into nanocarriers to enhance uptake by professional APCs with less proteolytic degradation and improved stability.[10,11] Furthermore, with coencapsulation of adjuvant, antigen-loaded NPs can induce *in situ* DC maturation and much stronger T cell responses. To date, the antigen delivery system mediated by nanocarriers have exhibited great potential in cancer immunotherapy.[6,8,10,11]

Many kinds of NP delivery systems have been developed for cancer chemotherapy and immunotherapy, including polymeric NPs, microspheres, liposomes, cell, or cell-derived vesicles, *etc.*[8,11−13] Among them, polymeric NPs, especially applying FDA-approved polymers (*e.g.*, poly(D,L-lactici-*co*-glycolic acid), PLGA) as a delivery system, have attracted much attention.[6,8,14] In our previous research, we have reported PLGA-NPs as melanoma-associated antigenic peptides, TRP2$_{180-182}$ and hgp100$_{25-33}$, delivery system. TRP2 peptide and toll-like receptor 4 agonist (MPLA) coentrapped PLGA-NPs are capable of promoting the presentation of antigen in APCs.[8] Recently, cell or cell-derived membrane vesicles have been proposed as potential drug delivery carriers, including erythrocytes (RBCs), macrophages, dendritic cells, stem cells, tumor cells, and so on.[13,15−18] Membrane vesicle-based drug delivery has received particular attention by virtue of their biological formation, antigenic components, and physicochemical properties.[19] For example, tumor cell-derived microparticles can be used as a good package of chemotherapeutic drugs, which exhibited anticancer activity with reduced adverse effects.[13] Compared with the above-mentioned cultured cell-derived vesicles, red blood cells (erythrocyte, RBCs) may be more appropriate for selective delivery of pharmacological agents because of their convenient isolation, intrinsic biocompatibility, and a variety of other remarkable properties.[15] Erythrocyte is an interesting tool for antigen delivery to target DC and induce CTL responses.[20−23] As an antigen carrier, RBCs can protect the antigens from blood clearance, deliver antigens in strategic organs, and present antigens directly to immune cells after processing by APCs.[23,24] The ovalbumin antigen entrapped-RBCs can promote the phagocytosis by APCs and result in the subsequent activation and proliferation of antigen-specific CD4$^+$ and CD8$^+$ effector T cells.[22] HIV regulatory protein, TAT conjugated on the RBC membrane exhibited a 1250-fold less dosage to induce a similar T-cell response compared with soluble TAT.[25] Several distinct methods

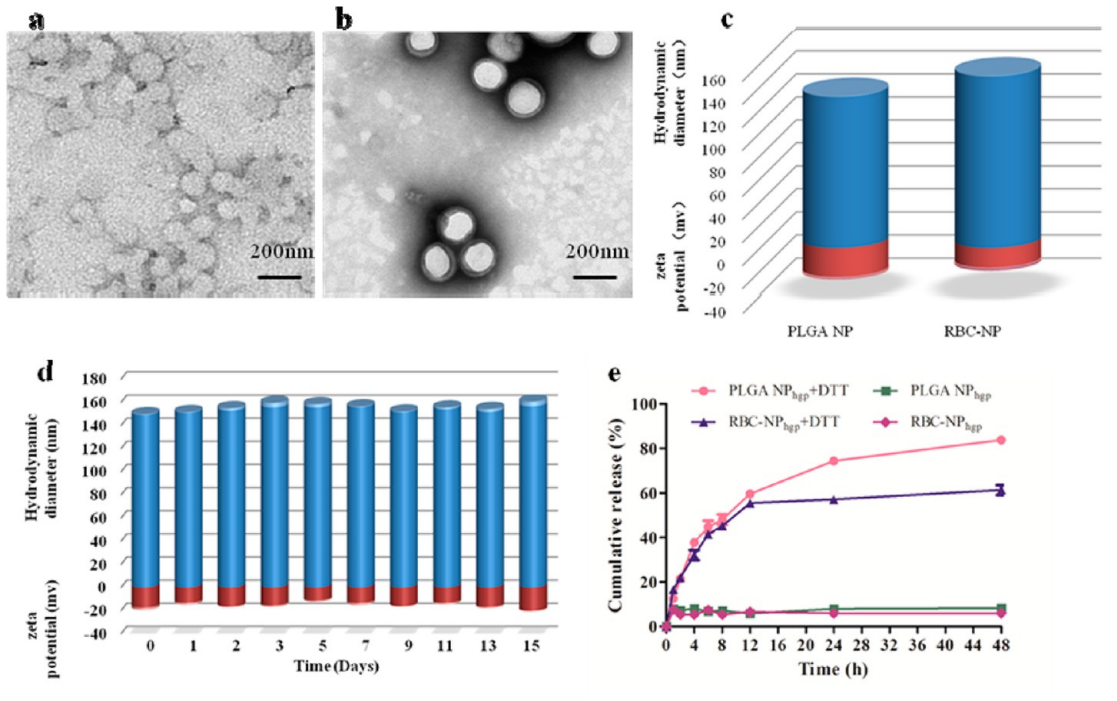

Figure 2. Characterizations of RBC-NP. TEM images of (a) PLGA-NPs and (b) RBC-NPs. Scale bar = 200 nm. (c) Hydrodynamic diameter (blue) and zeta potential (red) of PLGA-NPs and RBC-NPs measured by DLS. (d) *In vitro* particles stability assay of RBC-NPs in 1·PBS over a span of 15 days. (e) *In vitro* release profile of hgp from PLGA-NP_{hgp} or RBC-NP_{hgp} with/without DTT in PBS.

have been developed to load antigen in RBCs or onto the outer surfaces by physical encapsulation or chemical conjugation. The amount of antigen or drug entrapped in RBCs is variable and the encapsulated substances leak rapidly from the RBCs by the mainly used osmosis-based method.[23,25] The electroporation and biotin−avidin−biotin bridge may cause the disruption of cell membrane and affect the functionalities of proteins in RBCs.[26] Recently, functionalizing synthetic NPs with natural RBC membranes has been developed to construct RBC-mimicking NPs. The RBC membrane-cloaked NPs have been developed as a carrier to extend drug circulation time in cancer chemotherapy and a safe vaccine to deliver pore-forming toxins to immune systems.[27,28] With this in mind, an alternative approach is to directly employ RBC membranes as building materials to construct antigen carriers.

In the present work, we proposed a novel antigenic peptide delivery system with erythrocyte membrane-enveloped PLGA-NPs. The nanocarriers will combine the loading capacity of PLGA-NPs and the natural intrinsic properties, easy modification with targeting ligand and insertion capacity for lipid-like adjuvant of MPLA in the membrane structure of RBC. The feasibility of polymeric NPs as peptide and adjuvant delivery has been reported to efficiently induce functional CTL specific to tumor-associated antigens.[7] Compared to the hydrophobic melanoma-associated antigenic peptide $TRP2_{180-182}$, $hgp100_{25-33}$ with high hydrophilicity can hardly be entrapped in PLGA-NPs by the double emulsification method with entrapment as low as 0.5%, which limited its application in vaccine formulations.[8] The conjugation of the cysteine-modified peptide with a polymer *via* disulfide bond may be an alternative solution with enhanced entrapment efficiency and inclination to cleave under the reductive condition of abundant γ-glutamyl-cysteinyl-glycine (GSH) in the intracellular milieu.[29,30] The bioreducible NPs have been shown to enhance vaccine-induced antibody production and $CD8^+$ T cell-mediated tumor cell lysis.[31] Therefore, PLGA-SS-hgp NPs (PLGA-NP_{hgp}) were fabricated with reductive-cleaved hgp100 (hgp) conjugation and the surface of NPs was further decorated with the RBC membrane (Figure 1). The mannose receptor (MR) is a carbohydrate-binding receptor expressed on macrophages, DCs, and nonvascular endothelium.[32] More importantly, it is a key molecule in antigen recognition.[33] The activation of MR can arouse the targeting of APCs. Mannose-modified NPs enhanced vaccine delivery into draining LNs and increased vaccine-induced antitumor immune responses.[34] DSPE-PEG-mannose (DSPE-PEG-Man) was thus incorporated into RBC membranes to generate DSPE-PEG-Man-inserted-RBCs (Man-RBC), which presumably would be able to actively target APCs in lymphatic organs. Here, we characterized PLGA-SS-hgp@RBC NPs (RBC-NP_{hgp}) and PLGA-SS-hgp@Man-RBC NPs (Man-RBC-NP_{hgp}) *in vitro* and *in vivo* to evaluate the nanovaccine formulations on melanoma immunotherapy.

RESULTS AND DISCUSSION

Preparation and Characterization of RBC membrane-enveloped PLGA-NPs (RBC-NPs). PLGA-SS-hgp was synthesized *via* a three-step reaction (Supporting Information, Figure S1). After activation of carboxylic acid terminated PLGA with NHS, 2-(pyridyldithio)-ethylamine (PDA) was introduced to synthesize PLGA−PDA intermediate. The pyridyl sulfide group of PLGA−PDA was then exchanged by cysteine-modified hgp peptide, hgp-SH (KVPRNQDWLC) to form PLGA-SS-hgp. The conjugation of hgp to PLGA was confirmed by ^{1}H NMR (Supporting Information, Figure S2). Four methyl protons of valine and leucine were used as characteristic peaks at 0.79−0.94 ppm. Protons of some peptide bonds and aromatic ring of tryptophan appeared at 6.80−8.50 ppm, while the peaks belonging to PDA disappeared at the same area. The response of PLGA-SS-hgp in reductive environment was evaluated under the condition of DL-dithiothreitol (DTT) and the hgp content was calculated by HPLC measurement. No retention peak of hgp was observed in the sample of PLGA-SS-hgp without DTT treatment in contrast to free hgp-SH or DTT treated samples (Supporting Information, Figure S3). These results confirmed the successful synthesis of PLGA-SS-hgp and reductive-cleavage behavior of the pure peptide under *in vitro* reductive environment.

RBC-NPs were fabricated by preparing the PLGA-NPs by nanoprecipitation, deriving RBC membrane vesicles from natural RBCs by hypotonic hemolysis, and coating the RBC-membrane onto the surface of PLGA-NPs by serial extrusion.[14,35] To visualize the structure of RBC-NPs, the particles were negatively stained with phosphotungstic acid and observed through transmission electron microscopy (TEM) (Figure 2a,b). A spherical core−shell structure was exhibited as expected in RBC-NPs (Figure 2b). Moreover, the average hydrodynamic diameter of RBC-NPs was increased from 131.3 ± 0.6 nm for PLGA-NPs to 149.2 ± 0.6 nm, with a slight increase of 17.9 nm (Figure 2c). The shell-structure and thickness detected in the transmission electron microscopy (TEM) images and increased particle size measured in dynamic light scattering (DLS) were in good agreement with the thickness of the bilayer structure of natural RBC membranes which is known to be 5−10 nm.[36] Man-RBC-NPs, RBC-NP$_{hgp}$, and Man-RBC-NP$_{hgp}$ were prepared in the similar way.

Physiological stability is a significant challenge in the application of NP. Designed for biomedical applications, we evaluated the stability of PLGA-NPs and RBC-NPs by suspending them in two commonly used biological media, pH 7.4 phosphate buffer solution (PBS), and pure fetal bovine serum (FBS). The particle size and the surface zeta potential were continuously monitored by dynamic light scattering (DLS) for 15 days in PBS. The hydrodynamic diameter of the RBC-NPs was slightly changed from 149.2 ± 0.6 nm to 156.6 ± 4.6 nm, the zeta potential decreased from −17.5 ± 2.0 mV to −20.1 ± 0.7 mV (Figure 1d). It seems that no significant change was observed in PBS for at least 15 days. For the serum stability, we shelved the RBC-NPs for 4 h in FBS to monitor the absorbance change at 560 nm.[35] Cross-linking between NPs would be expected to happen if serum proteins bind to the surface of the NPs.[37] It is well-known that larger particles induce higher light scattering. Aggregation of unstable particles can thus be assessed by monitoring the increase in absorbance value.[35] The results suggested that RBC-NPs were more stable than PLGA-NPs in serum as there were no observable changes in absorbance within 4 h (Supporting Information, Figure S4).

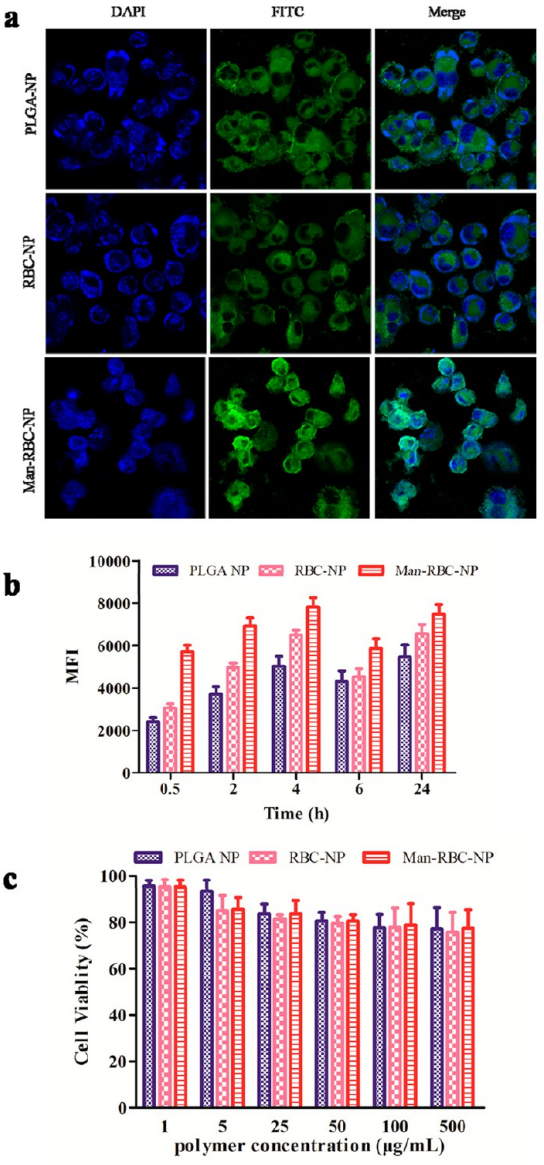

Figure 3. Cell uptake capability and cytotoxicity of RBC-NPs in DC2.4 cells. (a) CLSM images and (b) fluorescence intensity of DC2.4 incubated with coumarin 6-loaded PLGA-NPs, RBC-NPs, and Man-RBC-NPs. (c) *In vitro* cytotoxicity of NPs against DC2.4 cells after treatmnt for 24 h.

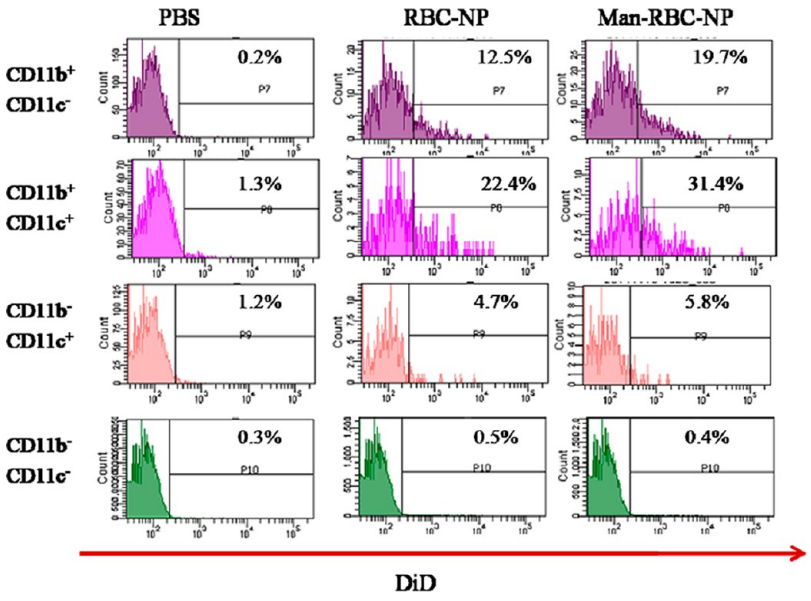

Figure 4. Uptake of DiD 6-loaded PLGA-NPs, RBC-NPs, and Man-RBC-NPs by APCs in the draining LNs *in vivo*. NPs were intradermally injected in the inguinal region of C57/BL6 mice. Cells were harvested from the draining LNs after 48 h, and then stained with anti-CD45R/B220, anti-CD11b, and anti-CD11c mAbs. The uptake of DiD-loaded NPs was assessed by flow cytometry.

This may occur because the RBC membrane-covered structure prevented the serum binding from RBC-NPs.

An important feature of the bioreducible NPs is that they are prone to cleavage in the presence of reductive agent, such as DTT, and then quickly releasing their cargoes. Accordingly, we evaluated the *in vitro* release profile of PLGA-NP_{hgp} and RBC-NP_{hgp} by coincubation with 10 mM DTT. As shown in Figure 2e, the PLGA-NP_{hgp} and RBC-NP_{hgp} showed controlled release behavior over 48 h, while negligible hgp release was detected in the absence of DTT. Moreover, RBC-NP_{hgp} exhibited slower sustained release of hgp compared with PLGA-NP_{hgp} in the presence of DTT which may be caused by the RBC barrier from this membrane-coated NP. It demonstrated that the bioreducible bond conjugated peptide-loaded NPs can realize preferentially intracellular stimuli-responsive release property instead of a burst release before uptake by DCs.

To ensure the retained membrane proteins of RBC in RBC-NPs after extrusion, SDS-PAGE analyses of Man-RBC-NPs along with PLGA-NPs, natural RBC membranes, Man-RBC, and RBC-NPs were performed in parallel (Supporting Information, Figure S5a). Compared to that of natural RBC membranes, the majority of protein content was not lost during the samples preparation. The protein profiles of Man-RBC-NPs and RBC-NPs were as similar as natural RBC membranes. To confirm the presence of specific antigens on the RBC-NPs, CD58 and CD59 were examined by Western blotting analysis, respectively. The results showed that CD58 and CD59 molecules both existed no matter the pre/post-membrane extrusion (Supporting Information, Figure S5b and S5c). CD59 is a small (20 kDa), globular, glycophosphatidyl inositol (GPI) linked glycoprotein on almost all tissues in the body and all circulating cells.[38] CD58 is a highly glycosylated cell adhesion molecule (55−70 kDa) that is expressed in diverse cell types as a transmembrane or GPI-membrane-anchored form.[39] CD58 and CD59 that distributed on the RBC surface are the corresponding ligands of CD2.[40] CD2 presents on the surface of T lymphocytes, which is a member of the immunoglobulin superfamily, and plays a crucial role in cell−cell adherence.[41] CD58 and CD59 are considered to play an important role in the interaction of T cells with target cells. Taken together, these observations suggested that RBC-NPs were stable enough to apply in biomedical conditions and the majority of membrane proteins were retained in RBC-NPs throughout the particle preparation process.

Man-RBC-NPs Enhance Cell Uptake and Promote Retention in Draining LNs. A key step by which naive T cells first become aware of tumor-associated antigens is the presentation of tumor antigens by host APCs. NPs (20−200 nm) are known to traffic to the draining LNs rapidly after intradermal injection where they are effectively taken up by resident DCs.[42] We supposed that the Man-RBC-NPs may efficiently home in on the LN when intradermally injected, because the NPs were small enough (<200 nm) to pass through the clefts and pores of lymphatic vessels. In light of the described functional features of DCs and their remarkable ability in cancer immunotherapy, the cell uptake capability of RBC-NPs and Man-RBC-NPs was investigated by confocal laser scanning microscope against DC2.4 cells, a DC line derived from C57/BL6 mice.[43] For the purpose of tracking and comparison, NPs were labeled with coumarin-6 (green). As shown in Figure 3a, after 2 h of exposure, all samples exhibited significant green

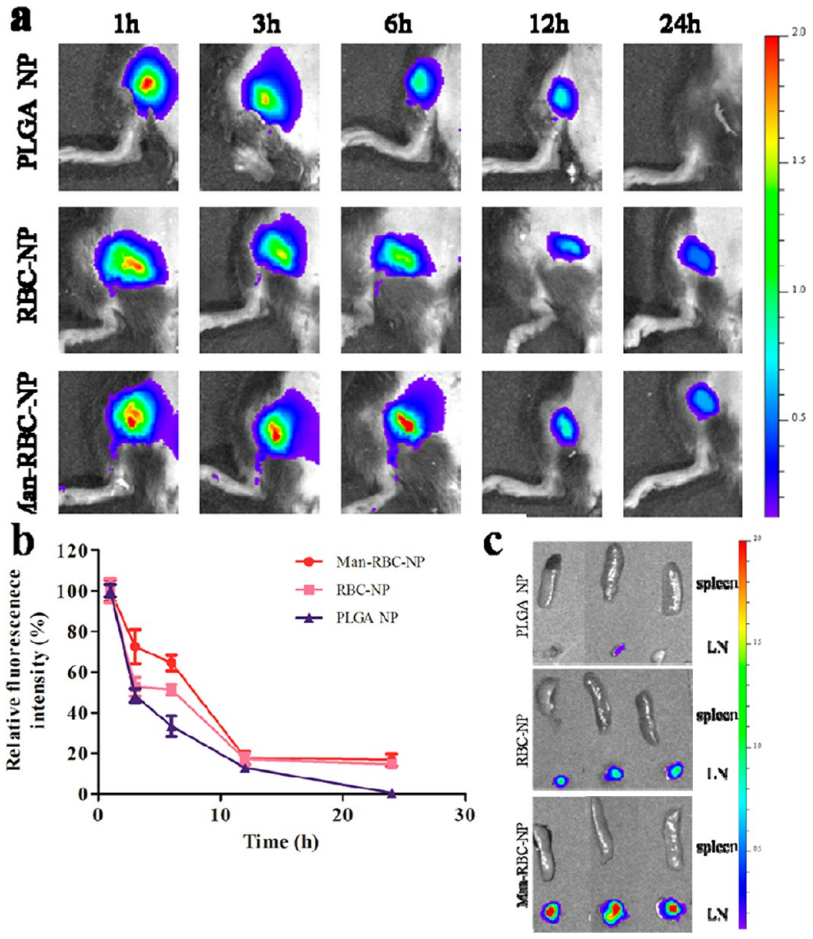

Figure 5. Antigen depot at the injection sites and antigen transport into draining LNs. C57/BL6 mice were intradermally injected in the hind legs with Cy5-labeled NPs. Antigen persistence at injection sites was evaluated and documented by an *in vivo* imaging system at the indicated time points. Living Image software was employed to quantify the fluorescence intensity at the injection sites. (a) Representative fluorescence images and (b) quantitative fluorescence intensity of antigen persistence at injection sites. (c) The image of LN and spleen at 24 h after intradermal injection.

fluorescence throughout the cytoplasm, which was closely located around the nuclei (blue) in DC2.4 cells. The results were further validated through quantitative assay by flow cytometry in Figure 3b. Both RBC-NPs and Man-RBC-NPs showed higher cell uptake capability compared with to PLGA-NPs. All samples reached the maximum cell uptake after 4 h of incubation. This suggested that Man-RBC-NPs and RBC-NPs have been effectively taken up by the DC2.4 cells. The enhanced cell uptake of Man-RBC-NPs was of immense benefit to cancer immunotherapy. Moreover, the negligible cytotoxicity of Man-RBC-NPs toward DC2.4 cells implied the high biocompatibility of our antigen delivery system (Figure 3c). To further uncover the possibility of Man-RBC-NPs being taken up by APCs, we injected lipid dye DiD-loaded NPs in the inguinal region of C57/BL6 mice to analyze the cellular populations in draining LN after 48 h of intradermal injection. As shown in Figure 4, RBC-NPs were positive in 22.4% of $CD11b^{+}CD11c^{+}$ DCs and 4.7% of $CD11b^{-}CD11c^{+}$ DCs. Also 19.7% of $CD11b^{+}CD11c^{-}$ macrophages took up the Man-RBC-NPs, whereas $CD11b^{-}CD11c^{-}$ cells did not. Man-RBC-NPs showed an increased uptake by $CD11b^{+}CD11c^{+}$ DCs, compared with RBC-NPs (31.4% vs 22.4%). These results suggested that Man-RBC-NPs and RBC-NPs can be efficiently taken up by APCs, including DCs and macrophages which make a vital contribution to immunity and inflammatory responses to pathogenic microorganisms.[44]

It is universally accepted that the ability to form a "depot effect" at the administration site contributes to the adjuvant effects of many antigen delivery systems. The antigen depot effect can extend the exposure time of antigens to the immune system, thereby enhancing antigen capture by the immunity system.[45] As mentioned above, RBC can act as an adjuvant. To explore the antigen depot effect of Man-RBC-NPs, mice were injected intradermally with Cy5-labeled RBC-NPs or Man-RBC-NPs to evaluate the maintenance of Cy5-labeled NPs at chosen time-points. As shown in Figure 5a and b, there was no fluorescent signal at the injection sites after 24 h injection with PLGA-NP. The fluorescent signal of Man-RBC-NPs was much higher than that of RBC-NPs, especially at 24 h after injection.

There was no significant difference between their decreasing rates of fluorescence intensity. To determine the precise localization of NPs, spleen and draining LNs were harvested 24 h later. The RBC-NPs and Man-RBC-NPs accumulated mostly in the draining LNs (Figure 5c). These facts indicated that Man-RBC-NPs have greater potential to target resident DCs and enhance the accumulation in the draining LNs through modification of the particles with mannose.

RBC-NP$_{hgp}$ Promotes the Expression of CD86 and Inflammatory Cytokines on DCs. DCs as professional APCs can stimulate both innate and adaptive immune responses.[46] The recognition and capture of tumor antigens by immature DCs is the first step in the cellular immune response. Meanwhile, maturated DCs with upregulation of costimulatory molecules (*e.g.*, CD40, CD80, CD86) may be necessary to induce T-cell responses.[47,48] Vaccine formulation is commonly composed of three key elements, antigens, adjuvants, and delivery system.[49] Although NPs can themselves act as an adjuvant in promoting DC maturation, choosing a potent adjuvant is also crucial.[50] The adjuvant has become a prerequisite in cancer vaccine design to induce potent immune responses *in vivo*.[49] PLGA-NPs carrying both the peptide antigen and an adjuvant MPLA had much stronger immune responses than other formulations, such as the peptide mixed with complete Freund's adjuvant (CFA).[8] Hence, we chose MPLA as adjuvant in the following vaccine formulations. It is an FDA-approved low-toxicity derivative of lipopolysaccharide (LPS) with immunostimulatory properties, which binds to toll-like receptor 4 (TLR-4). MPLA was incorporated with NPs at 0.1 wt % of the polymer weight by gently agitating the sample in a bath sonicator.[51] The ability of RBC-NPs to deliver tumor antigens and induce bone marrow-derived dendritic cells (BMDCs) maturation was tested by incubating different vaccine formulations with DCs derived from C57/BL6 mice. To monitor DC maturation, we focused on the expression of costimulatory molecule, CD86 and secretion of cytokines.[49] Data presented in Figure 6a showed that the percentage of CD86$^+$ cells in the Man-RBC-NP$_{hgp}$ treated group reached up to 81.6%. Compared with 33.1% CD86$^+$ cells in PBS, all vaccine formulations caused an up-regulation of CD86 expression. Moreover, the cytokines secretion is essential in the induction of antitumor immunity.[52] To confirm the function of RBC-NPs on the antigen presentation process, supernatants recovered from 24 h of incubation of BMDCs with vaccine formulations were tested by enzyme linked immunosorbent assay (ELISA) kits for secretion of tumor necrosis factor-α (TNF-α), interleukin-12(p70) (IL-12p70), and interferon-γ (IFN-γ). TNF-α and IFN-γ appear necessary for the inhibition of tumor, while IL-12 is a T-cell growth and stimulating factor and known to be a strong inducer of IFN-γ production. These cytokines are frequently analyzed to characterize antigen delivery efficiency to APCs from antigen-entrapped

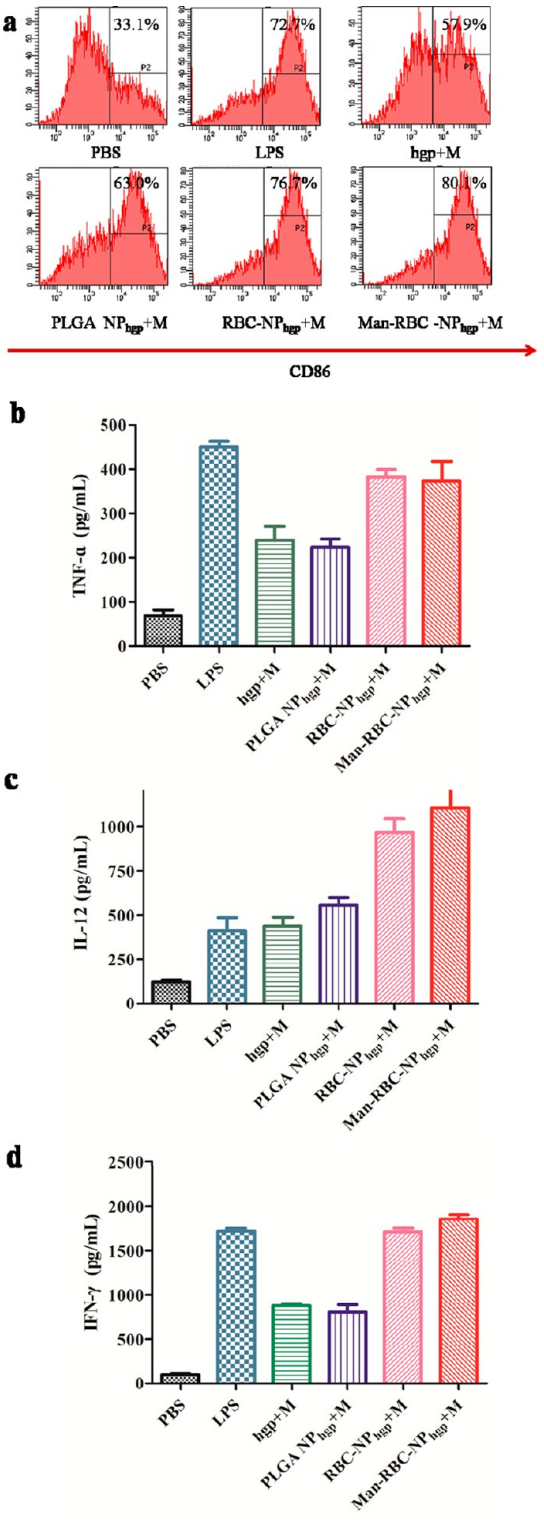

Figure 6. DC maturation induced by combination Man-RBC-NP$_{hgp}$ with MPLA *in vitro*. (a) CD86 as a maturation marker and analyzed by flow cytometry. Secretion of (b) TNF-α, (c) IL-12 P70, and (d) IFN-γ from BMDCs treated with different formulations.

NPs.[53] RBC-NP$_{hgp}$ and Man-RBC-NP$_{hgp}$ demonstrated the similarly increased cytokines secretion pattern as LPS compared to that of PBS and around 2-fold enhancement compared to those of free peptide+MPLA

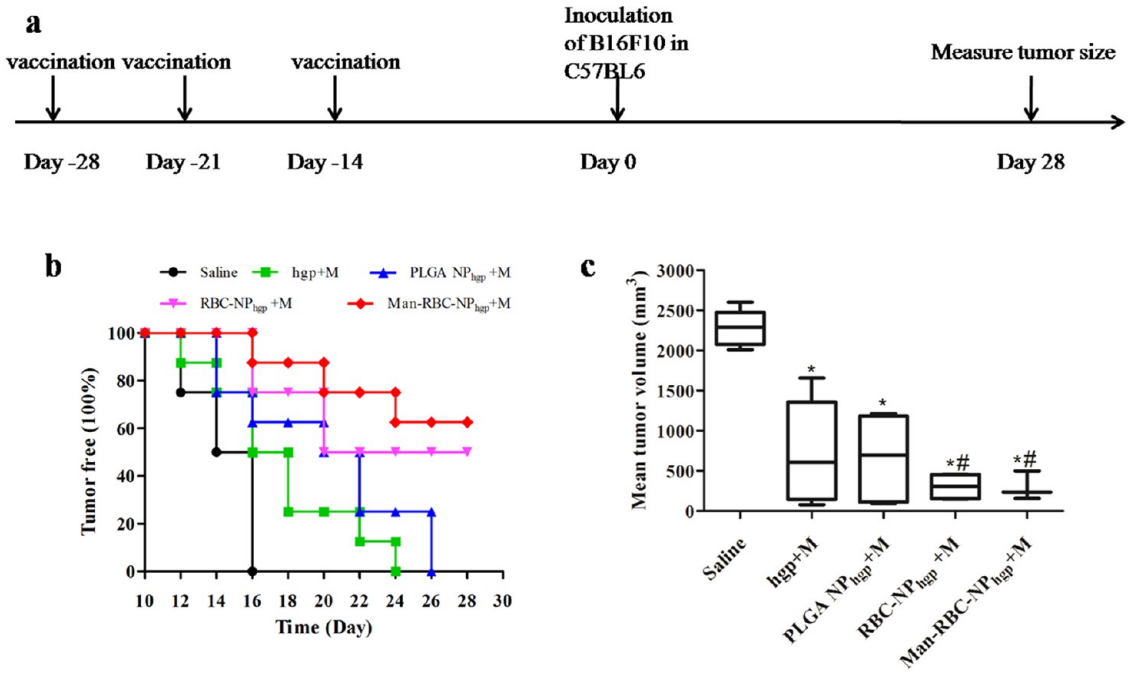

Figure 7. Efficacy of Man-RBC-NP$_{hgp}$ for tumor occurrence *in vivo*. Mice were immunized three times at 1 week interval with different vaccine formulations. After 14 days of the last immunization, B16F10 melanoma cells (5×10^4 cells) were subcutaneously injected. (a) The immunization protocol; (b) percentage of tumor free mice after tumor challenge; (c) tumor volume at day 28 after tumor cell challenge. Significant difference vs saline group (∗, $p < 0.05$). Significant difference vs hgp+M group (#, $p < 0.05$).

(hgp+M) and PLGA-NP$_{hgp}$+M (Figure 6b–d). Combined with the *in vitro* and *in vivo* results presented in Figures 3 to 6, targeted Man-RBC-NPs exhibited the superiority of DC uptake and activation compared with nontargeted RBC-NPs, PLGA-NPs and free hgp.

Man-RBC-NP$_{hgp}$ as Vaccine Induces the Preventive Effect on Tumor Occurring from the Prophylactic Model. To investigate the protective efficacy of the nanovaccine against B16F10 melanoma, vaccine formulations including hgp+M, PLGA-NP$_{hgp}$+M, RBC-NP$_{hgp}$+M, and Man-RBC-NP$_{hgp}$+M were immunized in B6 mice for three times with a 1 week interval (Figure 7a). Fourteen days after the last vaccination, B6 mice were inoculated with 5×10^4 B16F10 cells subcutaneously (SC). As shown in Figure 7b, all control mice (saline group) showed the palpable tumor at day 16. In contrast, the tumor-free time was prolonged to day 24 and 26 for hgp+M and PLGA-NP$_{hgp}$+M, respectively. Remarkably, the tumor occurring was retarded by immunization with Man-RBC-NP$_{hgp}$+M and RBC-NP$_{hgp}$+M. The percentages of tumor-free mice were 50% (four of eight mice) for RBC-NP$_{hgp}$+M and increased to 62.5% (five of eight mice) for Man-RBC-NP$_{hgp}$+M at day 28. Man-RBC-NP$_{hgp}$ and RBC-NP$_{hgp}$ also presented a preventive effect on tumor growth as demonstrated from Figure 7c for the tumor size measured at day 28. Compared with 2276.7 ± 223.6, 753.3 ± 647.5, and 693.2 ± 475.4 mm^3 for saline, hgp+M, and PLGA-NP$_{hgp}$+M, respectively, the mean tumor volumes of RBC-NP$_{hgp}$+M and Man-RBC-NP$_{hgp}$+M immunized mice were 295.8 ± 179.6 and 305.1 ± 166.6 mm^3, respectively ($p < 0.05$). Moreover, the tumor-free mice at day 28 were continuously observed. The tumor-free time was prolonged to day 42 and 38 for Man-RBC-NP$_{hgp}$+M and RBC-NP$_{hgp}$+M, respectively. The tumors occurring in these immunized mice were still growing and not completely cleared. It may be because the antitumor T cells become less responsive and their enduring activity is abrogated by the immunosuppressive DCs at advanced stages.[54] The immune checkpoint blockade or other combined therapy may be further developed to inhibit this cancer-induced immunosuppression. It seems that the nanovaccine developed can retard the tumor occurring, but cannot clear the tumor altogether.

Antitumor Efficacy in Xenograft Tumor Model by Man-RBC-NP$_{hgp}$. The antitumor efficacy of Man-RBC-NP$_{hgp}$ was further investigated on a SC xenograft B16F10 melanoma model. The tumor size and body weight were monitored every other day for 21 days after treated with above-mentioned vaccine formulations. The tumor-bearing mice were sacrificed as some of the tumors reached 20 mm in one dimension. No significant fluctuation of body weight was observed in any of the groups (Supporting Information, Figure S6a), indicating none obvious toxicity from the formulations. As shown in Figure 8a, both hgp+M and PLGA-NP$_{hgp}$+M showed a minor tumor inhibition effect. When compared with the saline, hgp, and PLGA-NP$_{hgp}$, both Man-RBC-NP$_{hgp}$+M and RBC-NP$_{hgp}$+M presented

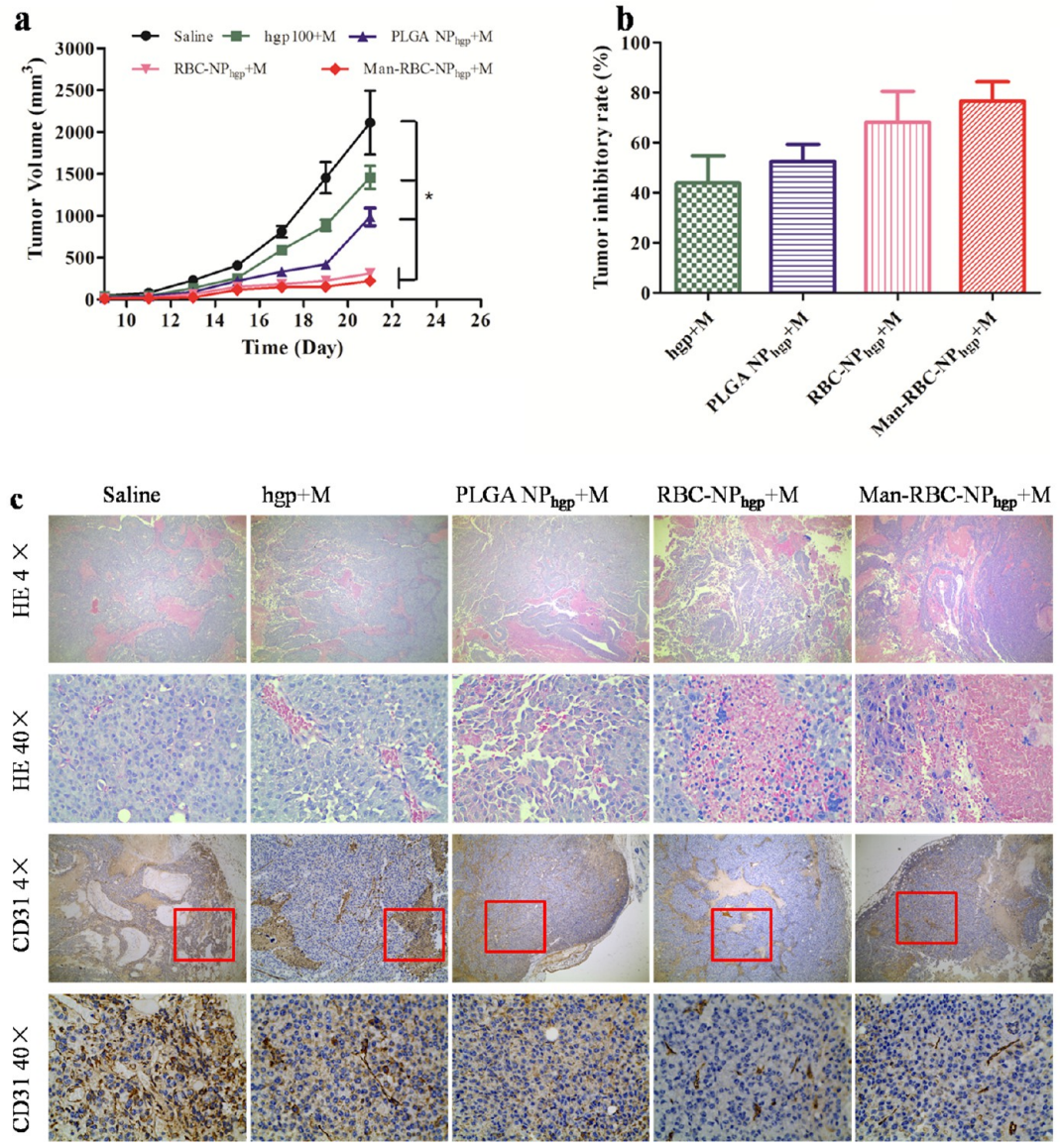

Figure 8. Antitumor activity of various formulations in B16F10 tumor model. (a) The tumor growth curves of B16F10 tumor-bearing mice model that were treated with different vaccine formulations (n = 6, $*$, $P < 0.05$). (b) Tumor inhibitory rate of different groups compared with saline. (c) Representative H&E staining sections and immunochemical staining of CD31 in tumor excised from tumor-bearing mice.

stronger suppression on tumor growth ($p < 0.05$). The average tumor volume of mice in Man-RBC-NP_{hgp}+M group was only about $^1/_5$ of that in saline group after 21 days. The rates of tumor growth inhibition from hgp+M, PLGA-NP_{hgp}+M, RBC-NP_{hgp}+M, and Man-RBC-NP_{hgp}+M were 43.9%, 52.6%, 68.2%, and 76.6%, respectively (Figure 8b). This was in good agreement with the isolated tumor images (Supporting Information, Figure S6b). The histopathology of tumor from the each group was investigated by H&E staining (Figure 8c). In saline group, the tumor tissue had a large obvious nucleus, with more nuclear division and less intercellular substance. In accordance with pathological features of melanoma, many melanin particles in the cytoplasm and less phenomenon of tumor tissue necrosis were also observed in the saline group. The groups injected with vaccine formulations showed varying degrees of tumor cell necrosis and intercellular substance increase. It was clear that cell nuclei apoptosis and the increased intercellular substance in RBC-NP_{hgp}+M and Man-RBC-NP_{hgp}+M were more severe as compared to other groups. The H&E results were consistent with variations of the tumor volume.

A tumor requires nutrients and oxygen *via* angiogenesis in the process of tumor growth and metastasis.[55] The major characteristic of tumor angiogenesis is the development of new blood vessels from the existing vasculature. CD31, a membrane protein constitutively expressed on the surface of endothelial cells of blood vessels, can quantify the microvessel density to measure angiogenesis.[56] To assess the progression of angiogeniesis in a B16F10 tumor, the tumor

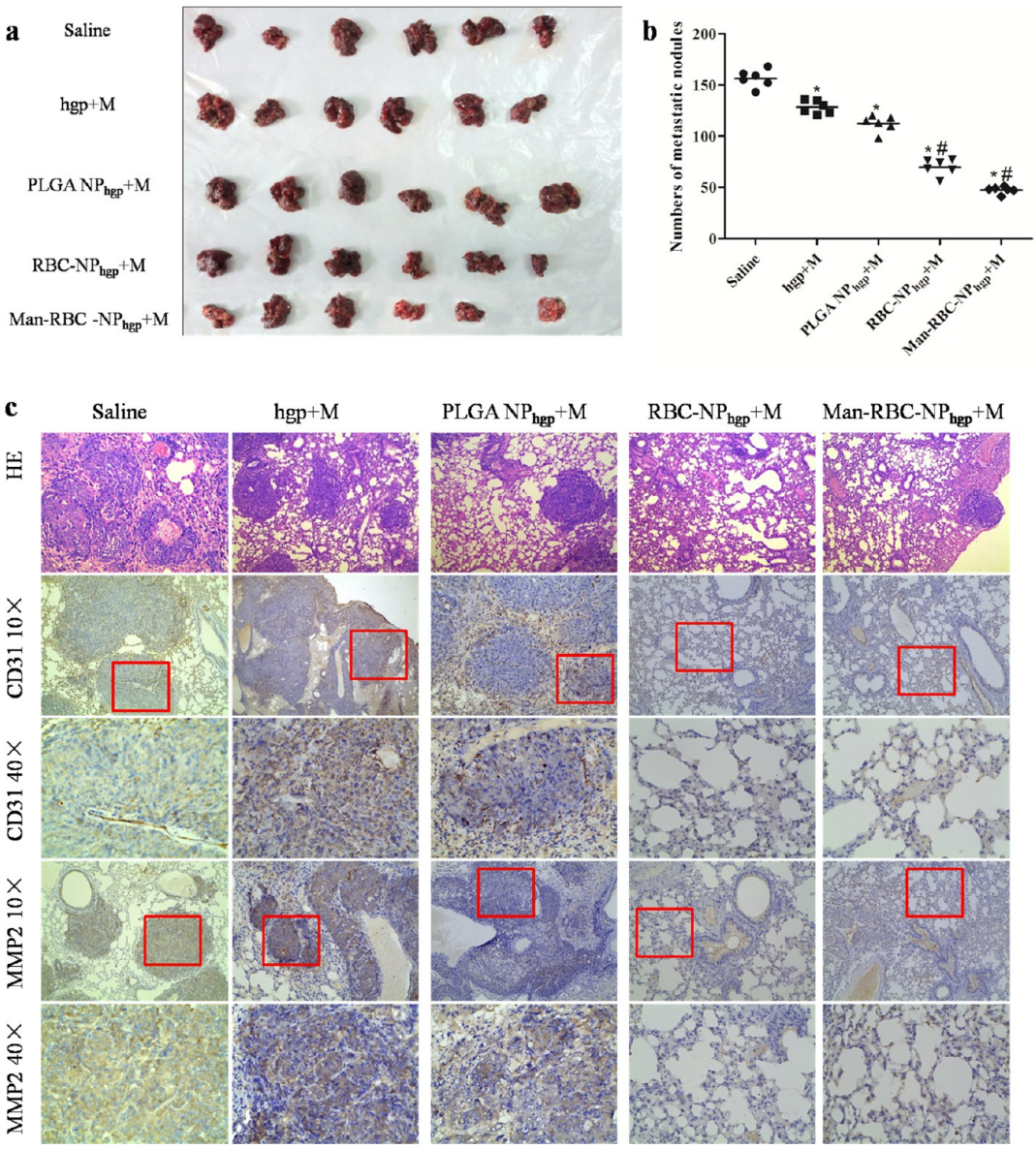

Figure 9. Inhibition of vaccine formulations in the B16F10 metastatic tumor model. (a) Lungs were harvested for imaging. (b) Tumor nodules exceeding 2 mm in diameter were counted manually. (c) Representative H&E staining sections showing the metastases of lungs and immunochemical staining was performed to detect the expression of CD31 and MMP-2 in lung. n = 6, significant difference vs saline group (∗, $p < 0.05$). significant difference vs hgp+M group (#, $p < 0.05$).

sections were immunohistochemically stained for CD31 (Figure 8c). Fewer CD31 positive cells were seen in the RBC-NP_{hgp} and Man-RBC-NP_{hgp} treated group compared with the other groups from the images in the striated skeletal muscle and the periphery of tumor. Blood vessels formed throughout the tumor in the control; therefore, the decreasing expression of CD31 would be beneficial to inhibit tumor growth.

The Inhibition of Tumor Metastasis with Man-RBC-NP_{hgp}. Melanoma is one of the most aggressive skin cancers with a high propensity to recurrence and metastasis. Metastasis is the leading cause of mortality in cancer patients. The lung was the most frequent site of metastases.[57] To test the suppressive effect of Man-RBC-NP_{hgp} on melanoma metastasis, mice were injected with B16F10 cells through the tail vein to establish the metastatic model. After that, C57/BL6 mice were treated on day 4 and 11 with tested formulations. Observable nodules (exceeding 2 mm in diameter) were found in all mice and counted manually. The significant pigmentation of migrated B16F10 cells in lung was easy to distinguish *via* photographs (Figure 9a). Compared with the other groups, significantly fewer metastasis nodules in the lung were developed after vaccination with Man-RBC-NP_{hgp}. The metastasis nodules counted by microscopy on the lungs of all groups presented a similar tendency as the isolated lung images (Figure 9b). The rates of nodules inhibition with hgp, PLGA-NP_{hgp}, RBC-NP_{hgp}, and Man-RBC-NP_{hgp} were 19.7%, 40.1%, 57.5%, and 70.5%, respectively

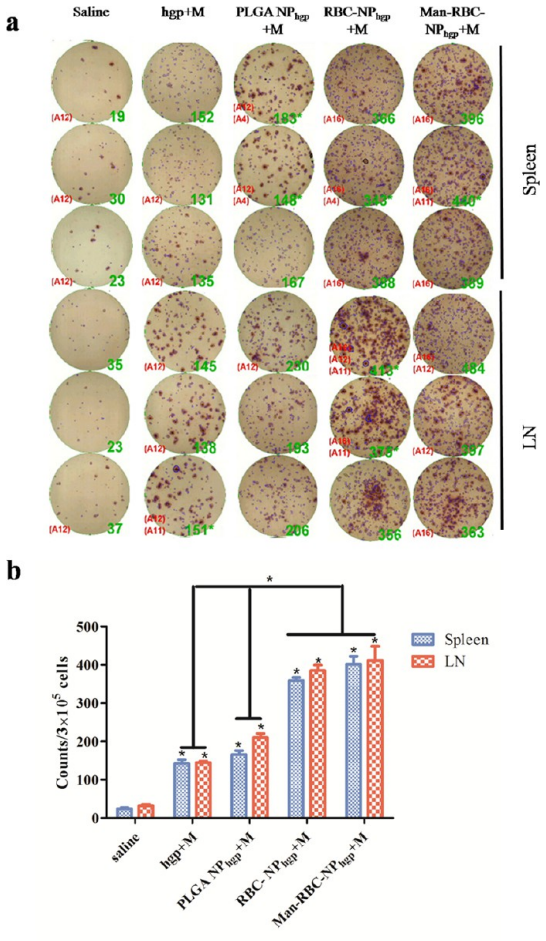

Figure 10. IFN-γ production from immunized mice. Spleen and draining LN were harvested 7 days after the last vaccination. Single cell suspension (3×10^5) was incubated with the indicated concentrations of hgp peptide for 30 h. IFN-γ production was measured with the ELISPOT assay system:. (a) representative spot and (b) the number of positive cells ($n = 3$, $*$, $p < 0.05$).

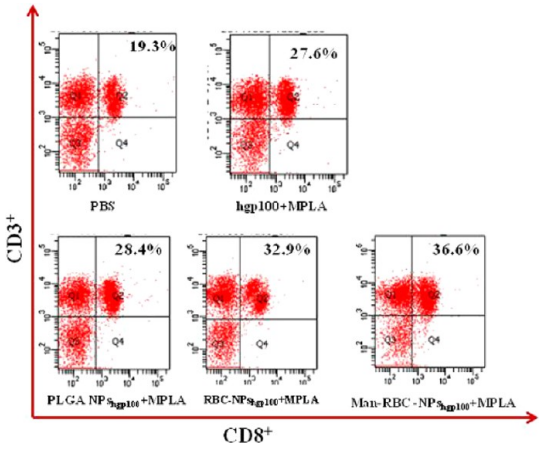

Figure 11. CTL response after vaccination in tumor-bearing mice. The cells of draining LNs isolated from immunized mice were stained with PE-Cy5 antimouse-CD3 and FITC-labeled anti-CD8 for 30 min at 4 °C in dark, and then analyzed using a flow cytometer.

(Supporting Information, Figure S7b). The metastasis was further visualized by H&E staining on lungs (Figure 8c), livers, and kidneys (Supporting Information, Figure S7c). Only a few nodules were seen from the lungs of RBC-NP$_{hgp}$ and Man-RBC-NP$_{hgp}$. No remarkable metastase nodules were observed from kidneys and livers.

The interaction between cancer cells and the extracellular cell matrix (ECM) is a key step during the procedure of metastasis.[58] ECM degradation, mediated by matrix metalloproteinases (MMPs), is a prerequisite for tumor metastasis. After degrading the ECM, tumor cells have the chance to migrate away from primary tumors and penetrate blood vessel walls.[59] MMPs, such as MMP-2 and MMP-9 are key enzymes involved in the metastatic process and have a primary effect on the ability of cancer cells to grow in a secondary site.[60] To further evaluate the suppression efficiency in the lung metastasis model, CD31 and MMP-2 expressions were studied through immunohistochemical staining (Figure 9c). Man-RBC-NP$_{hgp}$ and RBC-NP$_{hgp}$ exhibited a decrease in the CD31 and MMP-2 expressions. The metastasis assay showed that Man-RBC-NP$_{hgp}$ and RBC-NP$_{hgp}$ resulted in a significant inhibition of tumor metastasis with fewer metastasis nodules, and the lower expressions of CD31 and MMP2 compared with the other groups.

IFN-γ Production by Splenocytes and LNs from Immunized Mice. The tumor growth inhibitions demonstrated above may be attributed to the antigen-specific immune responses induced by Man-RBC-NPs containing both the antigenic peptide and adjuvant. IFN-γ is a key cytokine in tumor immunology, and positively associated with tumor rejection. The mechanism of IFN-γ-mediate antitumor immunity has been evidenced through plenty of studies.[61] IFN-γ plays an important role in the coordinating tumor immune responses, and the typical feature of activated T-cells is robust production of IFN-γ. To determine the frequency of activated T-cells, an IFN-γ-ELISPOT assay was used. The generation of discrete spots reflected the number of cytokine-secreting cells. Therefore, the spleen and draining LNs of B6 were extracted and processed into single cell suspensions on the seventh day after the last vaccination. As presented in Figure 10, the frequencies of IFN-γ secreting in the spleen and LNs immunized with RBC-NP$_{hgp}$ and Man-RBC-NP$_{hgp}$ were significantly higher than those of other formulations ($p < 0.05$). Man-RBC-NP$_{hgp}$ increased the IFN-γ spots up to 411 ± 64 per 3×10^5 LN cells which was 13.0, 2.8, 2.0, and 1.1-fold compared with those of saline, hgp+M, PLGA-NP$_{hgp}$+M, and RBC-NP$_{hgp}$+M, respectively. There was no significant difference between levels in the spleen and draining LN. Moreover, a significant difference was observed among hgp+M, PLGA-NP$_{hgp}$+M, and Man-RBC-NP$_{hgp}$+M treated groups ($p < 0.05$). The result was consistent with previous animal experiments.

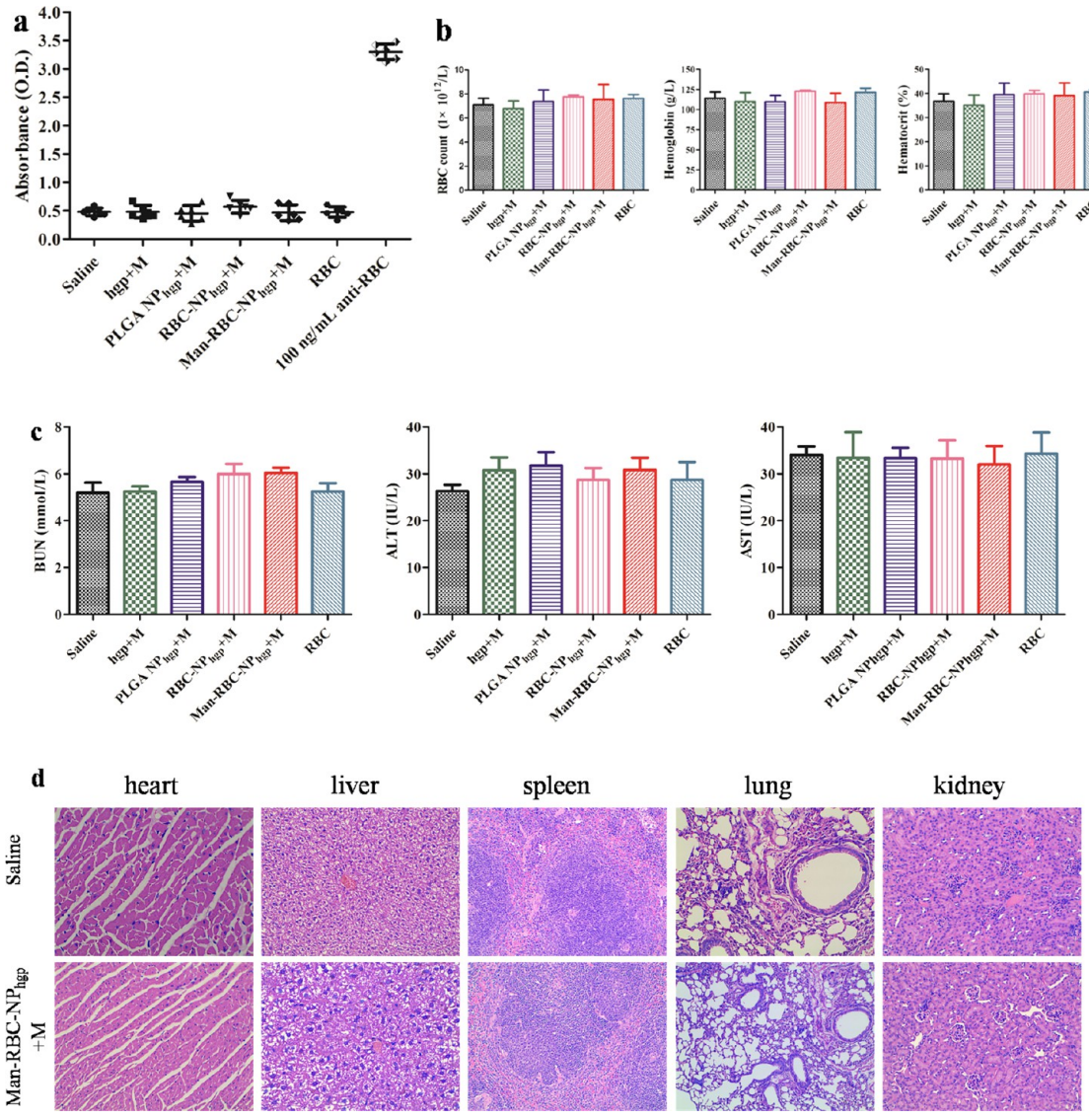

Figure 12. Anti-RBC titer assay and blood parameters monitoring of as-designed nanovaccine. (a) The anti-RBC titer was measured by ELISA at 3 weeks after the last immunization. (b) Monitoring of RBC count, hemoglobin level, and hematocrit of mice after different vaccinations. (c) Serum chemistry levels including blood urea nitrogen (BUN), alanine aminotransferase (ALT), and aspartate aminotransferase (AST) in mice after treatment with different vaccine formulations. (d) Representative H&E staining of mice organs after treatment with vaccine formulations. (b−d) The samples were collected at 7 days after last vaccine injection.

Man-RBC-NP$_{hgp}$ Enhance CTL Responses. A potential mechanism behind the remarkable immune response from the Man-RBC-NP$_{hgp}$ may be due to the antigen-specific CD8$^+$ T cells that generate CTL to reject cancer cells. CTL responses are important arms of antitumor immune responses.[62] The major effective strategy for cancer immunotherapy is to recognize antigens by tumor-specific CTL. To examine the immune responses to vaccines *in vivo*, the draining LNs of tumor-bearing mice were collected and stained with CD8 and CD3e. As shown in Figure 11, vaccinations with either RBC-NP$_{hgp}$ or Man-RBC-NP$_{hgp}$ led to a significant proliferation in CTL. Taking Man-RBC-NP$_{hgp}$ for example, the percentages of CTL could climb up to 36.6%, which is higher than 27.6% and 28.4% for hgp+M and PLGA-NP$_{hgp}$+M, respectively. The augmented CTL responses could be due to the enhancement of IFN-γ production. Over all, RBC-NP$_{hgp}$ and Man-RBC-NP$_{hgp}$ enhanced vaccine-induced CTL responses much more effectively than other vaccine formulations did, demonstrating the feasibility of RBC in antitumor immunity and providing us a deeper insight into the immunotherapy. In all, vaccinations utilizing RBC coated onto PLGA-NPs resulted in two distinct phases of immune responses *in situ*. First, innate responses included APC uptake and DC activation. In the second phase adaptive T-cell responses maintained a persistent CTL response. These results highlighted the benefit of augmenting immune cell responses vaccination with this nanovaccine.

Man-RBC-NP$_{hgp}$ Does Not Elicit Autoimmune Antibodies against RBCs. To evaluate whether the RBC membrane-coated NPs led to the induction of anti-RBC autoimmunity, we measured the autologous anti-RBC titers in serum of mice at 3 weeks after the last immunization using a well-documented ELISA method.[63] None of the serum samples from different vaccine formulations showed a significant increase in optical absorbance when compared with saline (Figure 12a). The absorbance values from the different vaccine formulations showed much less than the positive control (100 ng/mL anti-RBC). The results showed no observable elevation of autologous anti-RBC responses in mice receiving nanovaccine treatment compared with the control. Moreover, the blood was collected to monitor the RBC count, hemoglobin level, hematocrit, and the levels of ALT, AST, and BUN in all groups. As shown in Figure 12b and c, they were all at the normal range. Besides, there were no obvious toxicities or inflammatory infiltrates in the histological sections of heart, liver, spleen, lung, and kidney (Figure 12d). The results demonstrated the safety of the nanovaccine.[64]

CONCLUSION

In this paper, we constructed a novel nanovaccine formulation composed of three key elements, antigenic peptide (hgp100$_{25-33}$), adjuvant MPLA, and delivery system of mannose-inserted-RBC-membrane coated PLGA-NP. The nanovaccine demonstrated the superiority to an ordinarily used vaccine formulation against tumor prevention, growth, and metastasis. This RBC membrane-coated NPs delivery system could combine the antigen entrapment and stimuli-responsive property from polymeric NPs and the antigen presentation and adjuvant features of RBCs with membrane surface and protein integrity. The investigations in this research may provide a novel strategy to develop a safe, effective, low-cost, and biomimetic vaccine formulation in the future.

MATERIALS AND METHODS

Materials. Details of the materials can be found in the Supporting Information.

Cell Line, Cell Culture, and Animals. Murine melanoma cell line B16F10 (syngeneic with C57BL/6) and DC2.4 cells were grown in RPMI 1640 medium supplemented with 10% fetal bovine serum, 100 IU/mL of penicillin, and 100 μg/mL of streptomycin in a humidified atmosphere incubator with 5% CO_2 at 37 °C.

Adult C57BL/6 mice were purchased from the Experimental Animal Center of Wuhan University, China. All mice were maintained under specific pathogen-free (SPF) condition in the Animal Center of Huazhong University of Science and Technology, China. The animals were maintained at 25 ± 1 °C and 60% ± 10% humidity under a 12-h light/dark cycle during the experiments. All animals were treated according to the regulations of Chinese law and the local Ethical Committee Quantita.

Preparation of RBC Membrane and Ligand-Inserted RBC Membrane. The RBC-membrane derived vesicles were prepared using hypotonic hemolysis previously reported.[35] Briefly, whole blood was collected from female C57BL/6 mice (6−8 weeks) with 20 uL of low molecular heparin solution per milliliter of blood for anticoagulation. After the whole blood was centrifuged at 3500 rpm for 10 min at 4 °C, the plasma and buffycoat were carefully removed. The resulting packed RBCs were washed once in cold 1·PBS. And then, 20 mL of 0.25·PBS was added for hemolysis through the hypotonic medium treatment in ice-bath for 2 h. The solution was centrifuged twice at 9000 rpm for 10 min to remove the released hemoglobin, and the light pink pellet was then resuspended in 1 × PBS. To form ligand-inserted RBC ghosts, the light pink solution was incubated with DSPE-PEG-Man for 30 min.[65] The RBC-membrane was prepared by extruding through a 200 nm polycarbonate porous membrane with an Avanti mini-extruder (Avanti Polar Lipids).

Preparation of PLGA-NPs. PLGA-NPs were prepared by the nanoprecipitation method. The PLGA polymer was first dissolved in acetone at a 5 mg/mL concentration, added dropwise to 20 mL deionized water, and then stirred overnight to evaporate the organic solvent. After removing large particles by 3000 rpm centrifugation for 10 min, the particles were collected by centrifugation at 12000 rpm for 30 min and redispersed in distilled water for use. Cy5-labeled PLGA-NPs were prepared by mixing Cy5-amine with the activated PLGA-NPs for 30 min and purified to remove the free molecules of Cy5-amine. PLGA-NPs loaded with the lipophilic dye DiD or coumarin-6 were fabricated in a similar way as the PLGA-NPs.

Preparation of RBC-Membrane-Coated PLGA-NPs. One mL of PLGA-NPs or PLGA-NP$_{hgp}$ was mixed with 100 μL of RBC-membrane from whole blood. The resultant mixture was subsequently extruded nine times through a 200 nm polycarbonate porous membrane using an Avanti mini-extruder to yield the RBC-membrane-fused PLGA-NPs or PLGA-NP$_{hgp}$ (RBC-NPs or RBC-NP$_{hgp}$).

Characterization of RBC-NPs. The hydrodynamic diameter and zeta potential of NPs suspended in 1·PBS were measured by dynamic light scattering (DLS) (Zeta Plus, Brookhaven Instruments, USA). The morphology of RBC-NPs was observed by transmission electron microscope (TEM, JEM-1230, Japan) at an accelerating voltage of 200 keV. The stability experiments of RBC-NPs in PBS were monitored by DLS. Serum stability tests were conducted according to a previous report at the indicated time points.[35] The PLGA-NPs and RBC-NPs were suspended in 100% FBS with a final NP concentration of 1 mg/mL, and the absorbance values were measured at 560 nm at different times to monitor the particle aggregation in the presence of FBS. The *in vitro* release profiles of NPs were determined by suspending PLGA-NP$_{hgp}$ and RBC-NP$_{hgp}$ in release medium with or without 10 mM DTT, respectively. At the assigned time intervals, the samples were analyzed by HPLC. The proteins retained on RBC-NPs compared with those on the natural RBC membranes were observed by SDS-PAGE. CD58 and CD59 on RBC-NPs were identified by Western Blot.[66]

The Cell Uptake and Cytotoxicity Study. The ability of cell uptake was assessed by flow cytometry (CLSM, Leica TCSNT1, Germany) and confocal microscopy (Becton Dickinson, San Jose, CA). The cell cytotoxicity was determined by the MTT assay. Details of the experiment can be found in the Supporting Information.

Antigen Persistence at Injection Site. To monitor antigen persistence at the injection site *in vivo*, PLGA-NPs were labeled with the near-infrared fluorescent dyes Cy5-amine ester. C57BL/6 mice were injected by intradermal in the hind legs with different vaccine formulations. Lymph nodes nearby the injection site were isolated for fluorescent imaging after 24 h injection. Fluorescent images were acquired at different time points postinjection using an IVIS Lumina XR system equipped with a 150-W quartz halogen lamp and a 1 mW power scanning laser (Caliper Life Sciences, Hopkinton, USA). The parameters were fixed with exposure time of 0.5 s, binning of 1, f/stop of 2 and

filter excitation/emission wavelength sets of 640/670 nm.[67] Acquired images were analyzed by Living Imaging software.

Generation of Mouse Bone Marrow-Derived Dendritic Cells (BMDCs). BMDCs were prepared as previously reported with a minor modification.[8] Briefly, the BMDCs collected from marrow cavities of femurs and tibias of mice were cultured in 24-well plates containing 1 mL of RPMI 1640 medium supplemented with 10% FBS, 100 mg/mL streptomycin, 100 IU/mL penicillin, 10 ng/mL GM-CSF, and 5 ng/mL IL-4 at 37 °C in a humidified 5% CO_2 humidified atmosphere. DC maturation was induced at day 7 treated with 1 μg/mL of LPS stimulation for 24 h.

Cell Surface Marker Expression and Cytokine Analysis. Flow cytometry analysis was performed to evaluate DC phenotype. Cells were resuspended in PBS containing 1% FBS, stained with goat anti-mouse antibody against CD86-PE for 30 min at 4 °C in dark, and then analyzed using a flow cytometer.

For quantitative measurement of TNF-α, IL-12p70, and IFN-γ in the medium released by the cultured cells, the supernatant derived from DC cultures was harvested and measured by ELISA analysis according to the manufacturer's instructions at the indicated time (MultiSciences Biotech Co., Ltd., Hangzhou, China).

Immunization and Tumor Cell Challenge Assay. C57BL/6 mice were divided into five experimental groups and immunized three times at an interval of 1 week by intradermal injections of 100 μL of different vaccine formulations (50 μL/hind leg) containing 50 μg of hgp and 10 μg of MPLA. Fourteen days later after the last vaccination, 5×10^4 B16F10 cells were transplanted subcutaneously into the right flank of mice. The tumor size was measured every other day using a caliper, and mice were euthanized when the length reached 20 mm^3. The tumor volume was calculated as 0.5 × length × $width^2$.

Therapeutic Assay. Tumor inhibition activity against a solid tumor model was evaluated. B16F10 cells (5×10^4) suspended in 0.1 mL physiological saline were injected subcutaneously at the right flank of each mice. After 8 days of transplantation, all the tumor-bearing mice were divided randomly into five vaccine formulations (six mice per group). On day 9, 13, and 17 after tumor cell implantation, various formulations were administered. The tumor size and body weight of each mouse were measured every other day. The tumor was stained with hematoxyline and eosine after the mice were sacrificed. The CD31 expression was investigated through the immunohistochemical staining.

Metastasis Inhibition Assay. The metastasis model was established to determine the effect of vaccines on tumor metastasis using female B6 mice (6−8 week, 14−18 g). B16F10 melanoma cells suspension (1×10^6/0.1 mL of saline) were injected intravenously *via* the caudal vein to the mice. The mice were randomly divided into five groups with different formulations. Twenty days later, animals were euthanized with CO_2. The lungs, kidneys, and spleens were excised by gross anatomy and photographed. Organs containing metastases were fixed in Bovin fixative solution, and sections were taken and stained with hematoxyline and eosine. The number of metastatic lung nodules (pigmented nodules at the surface of the lung) was counted. The CD31 and MMP-2 expressions were investigated through the immunohistochemical staining.

IFN-γ ELISPOT Assay. To investigate the effect of various formulations on antigen-specific T-cell responses by IFN-γ ELISPOT assay, spleens and LNs were collected from mice on day 7 after last immunization. A 100 μL cell suspension (3×10^6 cell/mL) was incubated with 10 μg of the indicated peptide for 20 h in 96-well ELISPOT plates. The well with 100 μL of medium was used as a negative control, while the 100 μL cell suspension with ConA was used as a positive control. The assay was done according to the protocol supplied by the manufacturer (Dakewei Biotech Company Ltd., Shenzhen, China). Spots were counted using an automated analyzer (Immunospot, Cellular Technology Ltd.).

The CTL Activity in Draining LNs. To analyze immune effector cells in tumor-bearing mice, the percentage of $CD3e^+CD8^+$ T lymphocytes in LNs were determined by flow cytometry. LNs were teased apart into single cell suspensions by pressing with a plunger of a syringe. After being washed with PBS for two times, the cells were stained with PE-Cy5 antimouse-CD3 and FITC-labeled anti-CD8 for 30 min at 4 °C in dark, and then analyzed using a flow cytometer.

Determination of Anti-RBC Antibody Production. The anti-RBC antibody productions in the serum of immunized mice were quantitatively determined by ELISA in accordance with the manufacturer's protocol. Briefly, 3 weeks after the last immunization, the serums were collected from all mice (six in each group), diluted 1:5 with sample diluents and added to the wells in duplicate (50 μL). Then, 50 μL of horseradish peroxidase-conjugated rabbit antimouse antibody was added to each well, and the plate was incubated for 60 min at 37 °C. The plate was washed three times with 200 μL of washing buffer and incubated with 3,3′,5,5′-tetramethylbenzidine substrate solution in the dark for 15 min at room temperature. The enzyme reaction was stopped by adding 50 μL of 2 M H_2SO_4 to each well, and the optical density of the plate at 450 nm was read using a microplate reader (Multiskan MK3, Thermo, USA).

The Blood Parameters of the Nanovaccine. Blood was sampled at the seventh day after the last vaccine injection. The RBC count, hemoglobin level, and hematocrit were determined by an automated hematology analyzer. BUN, ALT, and AST were measured according to the manufacture's instruction (Nanjing Jiangcheng Bioengineering Institute, China) using a semiautomatic biochemical analyzer. Also, organs (heart, liver, spleen, lung, and kidney) were fixed in paraformaldehyde fixative solution, and sections were taken and stained with hematoxyline and eosine.

Statistical Analysis. Statistical analysis was performed using a two-tailed Student's *t* test by comparing with the control group unless specified with markings. The differences were considered statistically significant with $p < 0.05$.

Conflict of Interest: The authors declare no competing financial interest.

Supporting Information Available: Materials, additional methods, figures and tables. The Supporting Information is available free of charge on the ACS Publications website at DOI: 10.1021/acsnano.5b01042.

Acknowledgment. This work was supported by National Basic Research Program of China (973 Program, 2012CB932501), the National Natural Science Foundation of China (81373360 and 21474086), the Doctoral Fund of Ministry of Education of China (20120142120093), the Fundamental Research Funds for the Central Universities (2014TS091), Chutian Scholar Award, and 2013 Youth Scholar Award of HUST. We thank the Analytical and Testing Center of Huazhong University of Science for performing the TEM.

REFERENCES AND NOTES

1. Kirkwood, J. M.; Butterfield, L. H.; Tarhini, A. A.; Zarour, H.; Kalinski, P.; Ferrone, S. Immunotherapy of Cancer in 2012. *Ca-Cancer J. Clin.* **2012**, *62*, 309–335.
2. Banchereau, J.; Steinman, R. M. Dendritic Cells and the Control of Immunity. *Nature* **1998**, *392*, 245–252.
3. Kantoff, P. W.; Ferrari, A. C.; Higano, C. S.; Shore, N. D.; Berger, E. R.; Small, E. J.; Penson, D. F.; Redfern, C. H.; Robert, D.; Sims, R. B.; et al. Sipuleucel-T Immunotherapy for Castration-Resistant Prostate Cancer. *N. Engl. J. Med.* **2010**, *363*, 411–422.
4. Kleindienst, P.; Brocker, T. Endogenous Dendritic Cells Are Required for Amplification of T Cell Responses Induced by Dendritic Cell Vaccines *in Vivo*. *J. Immunol.* **2003**, *170*, 2817–2823.
5. Ali, O. A.; Huebsch, N.; Cao, L.; Dranoff, G.; Mooney, D. J. Infection-Mimicking Materials to Program Dendritic Cells *in Situ*. *Nat. Mater.* **2009**, *8*, 151–158.
6. Tan, S.; Sasada, T.; Bershteyn, A.; Yang, K.; Ioji, T.; Zhang, Z. Combinational Delivery of Lipid-Enveloped Polymeric Nanoparticles Carrying Different Peptides for Anti-Tumor Immunotherapy. *Nanomedicine (London, U. K.)* **2014**, *9*, 635–647.
7. Krishnamachari, Y.; Geary, S. M.; Lemke, C. D.; Salem, A. K. Nanoparticle Delivery Systems in Cancer Vaccines. *Pharm. Res.* **2011**, *28*, 215–236.

8. Zhang, Z.; Tongchusak, S.; Mizukami, Y.; Kang, Y. J.; Ioji, T.; Touma, M.; Reinhold, B.; Keskin, D. B.; Reinherz, E. L.; Sasada, T. Induction of Anti-Tumor Cytotoxic T Cell Responses through PLGA-Nanoparticle Mediated Antigen Delivery. *Biomaterials* **2011**, *32*, 3666–3678.
9. Lee, I. H.; Kwon, H. K.; An, S.; Kim, D.; Kim, S.; Yu, M. K.; Lee, J. H.; Lee, T. S.; Im, S. H.; Jon, S. Imageable Antigen-Presenting Gold Nanoparticle Vaccines for Effective Cancer Immunotherapy *in Vivo*. *Angew. Chem., Int. Ed.* **2012**, *51*, 8800–8805.
10. Shen, H.; Ackerman, A. L.; Cody, V.; Giodini, A.; Hinson, E. R.; Cresswell, P.; Edelson, R. L.; Saltzman, W. M.; Hanlon, D. J. Enhanced and Prolonged Cross-Presentation Following Endosomal Escape of Exogenous Antigens Encapsulated in Biodegradable Nanoparticles. *Immunology* **2006**, *117*, 78–88.
11. Langer, R.; Cleland, J. L.; Hanes, J. New Advances in Microsphere-Based Single-Dose Vaccines. *Adv. Drug Delivery Rev.* **1997**, *28*, 97–119.
12. Xiang, S. D.; Scalzo-Inguanti, K.; Minigo, G.; Park, A.; Hardy, C. L.; Plebanski, M. Promising Particle-Based Vaccines in Cancer Therapy. *Expert Rev. Vaccines* **2008**, *7*, 1103–1119.
13. Tang, K.; Zhang, Y.; Zhang, H.; Xu, P.; Liu, J.; Ma, J.; Lv, M.; Li, D.; Katirai, F.; Shen, G. X.; et al. Delivery of Chemotherapeutic Drugs in Tumour Cell-Derived Microparticles. *Nat. Commun.* **2012**, *3*, 1282.
14. Govender, T.; Stolnik, S.; Garnett, M. C.; Illum, L.; Davis, S. S. PLGA Nanoparticles Prepared by Nanoprecipitation: Drug Loading and Release Studies of a Water Soluble Drug. *J. Controlled Release* **1999**, *57*, 171–185.
15. Hu, C. M.; Fang, R. H.; Zhang, L. Erythrocyte-Inspired Delivery Systems. *Adv. Healthcare Mater.* **2012**, *1*, 537–547.
16. Choi, M. R.; Stanton-Maxey, K. J.; Stanley, J. K.; Levin, C. S.; Bardhan, R.; Akin, D.; Badve, S.; Sturgis, J.; Robinson, J. P.; Bashir, R.; et al. A Cellular Trojan Horse for Delivery of Therapeutic Nanoparticles into Tumors. *Nano Lett.* **2007**, *7*, 3759–3765.
17. Tian, X.; Zhu, M.; Tian, Y.; Ramm, G. A.; Zhao, Y.; Nie, G. A Membrane Vesicle-Based Dual Vaccine against Melanoma and Lewis Lung Carcinoma. *Biomaterials* **2012**, *33*, 6147–6154.
18. Roger, M.; Clavreul, A.; Venier-Julienne, M. C.; Passirani, C.; Sindji, L.; Schiller, P.; Montero-Menei, C.; Menei, P. Mesenchymal Stem Cells as Cellular Vehicles for Delivery of Nanoparticles to Brain Tumors. *Biomaterials* **2010**, *31*, 8393–8401.
19. Tan, S.; Wu, T.; Zhang, D.; Zhang, Z. Cell or Cell Membrane-Based Drug Delivery Systems. *Theranostics* **2015**, *5*, 863–881.
20. Chiarantini, L.; Argnani, R.; Zucchini, S.; Stevanato, L.; Zabardi, P.; Grossi, M. P.; Magnani, M.; Manservigi, R. Red Blood Cells as Delivery System for Recombinant HSV-1 Glycoprotein B: Immunogenicity and Protection in Mice. *Vaccine* **1997**, *15*, 276–280.
21. Dominici, S. Red Blood Cell-Mediated Delivery of Recombinant HIV-1 Tat Protein in Mice Induces Anti-Tat Neutralizing Antibodies and CTL. *Vaccine* **2003**, *21*, 2073–2081.
22. Banz, A.; Cremel, M.; Rembert, A.; Godfrin, Y. *In Situ* Targeting of Dendritic Cells by Antigen-Loaded Red Blood Cells: A Novel Approach to Cancer Immunotherapy. *Vaccine* **2010**, *28*, 2965–2972.
23. Cremel, M.; Guerin, N.; Horand, F.; Banz, A.; Godfrin, Y. Red Blood Cells as Innovative Antigen Carrier to Induce Specific Immune Tolerance. *Int. J. Pharm.* **2013**, *443*, 39–49.
24. Godfrin, Y.; Horand, F.; Cremel, M. Can Red Blood Cells Prove to Be a Useful Tool in Tumor Immunotherapy? *Immunotherapy* **2012**, *4*, 871–873.
25. Corinti, S.; Chiarantini, L.; Dominici, S.; Laguardia, M. E.; Magnani, M.; Girolomoni, G. Erythrocytes Deliver Tat to Interferon-Gamma-Treated Human Dendritic Cells for Efficient Initiation of Specific Type 1 Immune Responses *in Vitro*. *J. Leukoc. Biol.* **2002**, *71*, 652–658.
26. Millan, C. G.; Marinero, M. L.; Castaneda, A. Z.; Lanao, J. M. Drug, Enzyme and Peptide Delivery Using Erythrocytes as Carriers. *J. Controlled Release* **2004**, *95*, 27–49.
27. Aryal, S.; Hu, C. M.; Fang, R. H.; Dehaini, D.; Carpenter, C.; Zhang, D. E.; Zhang, L. Erythrocyte Membrane-Cloaked Polymeric Nanoparticles for Controlled Drug Loading and Release. *Nanomedicine (London, U. K.)* **2013**, *8*, 1271–1280.
28. Hu, C. M.; Fang, R. H.; Luk, B. T.; Zhang, L. Nanoparticle-Detained Toxins for Safe and Effective Vaccination. *Nat. Nanotechnol.* **2013**, *8*, 933–938.
29. Hirosue, S.; Kourtis, I. C.; van der Vlies, A. J.; Hubbell, J. A.; Swartz, M. A. Antigen Delivery to Dendritic Cells by Poly(Propylene Sulfide) Nanoparticles with Disulfide Conjugated Peptides: Cross-Presentation and T Cell Activation. *Vaccine* **2010**, *28*, 7897–7906.
30. Meng, F.; Hennink, W. E.; Zhong, Z. Reduction-Sensitive Polymers and Bioconjugates for Biomedical Applications. *Biomaterials* **2009**, *30*, 2180–2198.
31. Li, P.; Luo, Z.; Liu, P.; Gao, N.; Zhang, Y.; Pan, H.; Liu, L.; Wang, C.; Cai, L.; Ma, Y. Bioreducible Alginate-Poly(Ethylenimine) Nanogels as an Antigen-Delivery System Robustly Enhance Vaccine-Elicited Humoral and Cellular Immune Responses. *J. Controlled Release* **2013**, *168*, 271–279.
32. Stahl, P. D.; Ezekowitz, R. A. B. The Mannose Receptor Is a Pattern Recognition Receptor Involved in Host Defense. *Curr. Opin. Immunol.* **1998**, *10*, 50–55.
33. Martinez-Pomares, L. The Mannose Receptor. *J. Leukocyte Biol.* **2012**, *92*, 1177–1186.
34. Sheng, K. C.; Kalkanidis, M.; Pouniotis, D. S.; Esparon, S.; Tang, C. K.; Apostolopoulos, V.; Pietersz, G. A. Delivery of Antigen Using a Novel Mannosylated Dendrimer Potentiates Immunogenicity *in Vitro* and *in Vivo*. *Eur. J. Immunol.* **2008**, *38*, 424–436.
35. Hu, C. M.; Zhang, L.; Aryal, S.; Cheung, C.; Fang, R. H.; Zhang, L. Erythrocyte Membrane-Camouflaged Polymeric Nanoparticles as a Biomimetic Delivery Platform. *Proc. Natl. Acad. Sci. U. S. A.* **2011**, *108*, 10980–10985.
36. Hochmuth, R.; Evans, C.; Wiles, H.; McCown, J. Mechanical Measurement of Red Cell Membrane Thickness. *Science* **1983**, *220*, 101–102.
37. Popielarski, S. R.; Hu-Lieskovan, S.; French, S. W.; Triche, T. J.; Davis, M. E. A Nanoparticle-Based Model Delivery System to Guide the Rational Design of Gene Delivery to the Liver. 2. *In Vitro* and *in Vivo* Uptake Results. *Bioconjugate Chem.* **2005**, *16*, 1071–1080.
38. Kimberley, F. C.; Sivasankar, B.; Paul Morgan, B. Alternative Roles for CD59. *Mol. Immunol.* **2007**, *44*, 73–81.
39. Challa-Malladi, M.; Lieu, Y. K.; Califano, O.; Holmes, A. B.; Bhagat, G.; Murty, V. V.; Dominguez-Sola, D.; Pasqualucci, L.; Dalla-Favera, R. Combined Genetic Inactivation of Beta2-Microglobulin and CD58 Reveals Frequent Escape from Immune Recognition in Diffuse Large B Cell Lymphoma. *Cancer Cell* **2011**, *20*, 728–740.
40. Takami, A.; Zeng, W. H.; Wang, H. B.; Matsuda, T.; Nakao, S. Cytotoxicity against Lymphoblastoid Cells Mediated by a T-Cell Clone from an Aplastic Anaemia Patient: Role of CD59 on Target Cells. *Br. J. Haematol.* **1999**, *107*, 791–796.
41. Zhao, Y. Z.; Jia, J.; Li, Y. B.; Guo, C. X.; Zhou, X. Q.; Sun, Z. W. Effects of Endosulfan on the Immune Function of Erythrocytes, and Potential Protection by Testosterone Propionate. *J. Toxicol. Sci.* **2014**, *39*, 701–710.
42. Manolova, V.; Flace, A.; Bauer, M.; Schwarz, K.; Saudan, P.; Bachmann, M. F. Nanoparticles Target Distinct Dendritic Cell Populations According to Their Size. *Eur. J. Immunol.* **2008**, *38*, 1404–1413.
43. Shen, Z.; Reznikoff, G.; Dranoff, G.; Rock, K. L. Cloned Dendritic Cells Can Present Exogenous Antigens on Both MHC Class I and Class II Molecules. *J. Immunol.* **1997**, *158*, 2723–2730.
44. Fogg, D. K.; Sibon, C.; Miled, C.; Jung, S.; Aucouturier, P.; Littman, D. R.; Cumano, A.; Geissmann, F. A Clonogenic Bone Marrow Progenitor Specific for Macrophages and Dendritic Cells. *Science* **2006**, *311*, 83–87.
45. Christensen, D.; Henriksen-Lacey, M.; Kamath, A. T.; Lindenstrom, T.; Korsholm, K. S.; Christensen, J. P.; Rochat, A. F.; Lambert, P. H.; Andersen, P.; Siegrist, C. A.; et al. A Cationic Vaccine Adjuvant Based on a Saturated Quaternary Ammonium Lipid Have Different *in Vivo* Distribution

Kinetics and Display a Distinct CD4 T Cell-Inducing Capacity Compared to its Unsaturated Analog. *J. Controlled Release* **2012**, *160*, 468–476.
46. Cella, M.; Sallusto, F.; Lanzavecchia, A. Origin, Maturation and Antigen Presenting Function of Dendritic Cells. *Curr. Opin. Immunol.* **1997**, *9*, 10–16.
47. Wang, Y. Q.; Wu, J.; Fan, Q. Z.; Zhou, M.; Yue, Z. G.; Ma, G. H.; Su, Z. G. Novel Vaccine Delivery System Induces Robust Humoral and Cellular Immune Responses Based on Multiple Mechanisms. *Adv. Healthcare Mater.* **2014**, *3*, 670–681.
48. Pasare, C.; Medzhitov, R. Toll Pathway-Dependent Blockade of $CD4^+CD25^+$ T Cell-Mediated Suppression by Dendritic Cells. *Science* **2003**, *299*, 1033–1036.
49. Dewitte, H.; Verbeke, R.; Breckpot, K.; De Smedt, S. C.; Lentacker, I. Nanoparticle Design to Induce Tumor Immunity and Challenge the Suppressive Tumor Microenvironment. *Nano Today* **2014**, *9*, 743.
50. Singh, M.; Chakrapani, A.; O'Hagan, D. Nanoparticles and Microparticles as Vaccine-Delivery Systems. *Expert Rev. Vaccines* **2007**, *6*, 797–808.
51. Fang, R. H.; Hu, C. M.; Luk, B. T.; Gao, W.; Copp, J. A.; Tai, Y.; O'Connor, D. E.; Zhang, L. Cancer Cell Membrane-Coated Nanoparticles for Anticancer Vaccination and Drug Delivery. *Nano Lett.* **2014**, *14*, 2181–2188.
52. Marrache, S.; Tundup, S.; Harn, D. A.; Dhar, S. *Ex Vivo* Programming of Dendritic Cells by Mitochondria-Targeted Nanoparticles to Produce Interferon-Gamma for Cancer Immunotherapy. *ACS Nano* **2013**, *7*, 7392–7402.
53. Hamdy, S.; Haddadi, A.; Shayeganpour, A.; Samuel, J.; Lavasanifar, A. Activation of Antigen-Specific T Cell-Responses by Mannan-Decorated PLGA Nanoparticles. *Pharm. Res.* **2011**, *28*, 2288–2301.
54. Scarlett, U. K.; Rutkowski, M. R.; Rauwerdink, A. M.; Fields, J.; Escovar-Fadul, X.; Baird, J.; Cubillos-Ruiz, J. R.; Jacobs, A. C.; Gonzalez, J. L.; Weaver, J.; et al. Ovarian Cancer Progression is Controlled by Phenotypic Changes in Dendritic Cells. *J. Exp. Med.* **2012**, *209*, 495–506.
55. Papetti, M.; Herman, I. M. Mechanisms of Normal and Tumor-Derived Angiogenesis. *Am. J. Physiol. Cell Physiol.* **2002**, *282*, C947–970.
56. Culp, W. D.; Neal, R.; Massey, R.; Egevad, L.; Pisa, P.; Garland, D. Proteomic Analysis of Tumor Establishment and Growth in the B16-F10 Mouse Melanoma Model. *J. Proteome Res.* **2006**, *5*, 1332–1343.
57. Hui, Q.; Yu, X.; Hui, Z.; Zuohua, F. Inhibition Growth and Metastasis of Melanoma by 4−1BBL Expressed in Normal Tissue Cells by Regulating the Function of Immune Cells. *Cancer Biother.Radiopharm.* **2009**, *24*, 597–605.
58. Pan, X.; Xiong, D.; Yao, X.; Xin, Y.; Zhang, L.; Chen, J. Up-Regulating Ribonuclease Inhibitor Inhibited Epithelial-to-Mesenchymal Transition and Metastasis in Murine Melanoma Cells. *Int. J. Biochem. Cell Biol.* **2012**, *44*, 998–1008.
59. Egeblad, M.; Werb, Z. New Functions for the Matrix Metalloproteinases in Cancer Progression. *Nat. Rev. Cancer* **2002**, *2*, 161–174.
60. Chambers, A. F.; Groom, A. C.; MacDonald, I. C. Dissemination and Growth of Cancer Cells in Metastatic Sites. *Nat. Rev. Cancer* **2002**, *2*, 563–572.
61. Dunn, G. P.; Koebel, C. M.; Schreiber, R. D. Interferons, Immunity and Cancer Immunoediting. *Nat. Rev. Immunol.* **2006**, *6*, 836–848.
62. Roth, C.; Rochlitz, C.; Kourilsky, P. Immune Response against Tumors. *Adv. Immunol.* **1994**, *57*, 281–351.
63. Mqadmi, A.; Zheng, X.; Yazdanbakhsh, K. $CD4^+CD25^+$ Regulatory T Cells Control Induction of Autoimmune Hemolytic Anemia. *Blood* **2005**, *105*, 3746–3748.
64. Copp, J. A.; Fang, R. H.; Luk, B. T.; Hu, C. M.; Gao, W.; Zhang, K.; Zhang, L. Clearance of Pathological Antibodies Using Biomimetic Nanoparticles. *Proc. Natl. Acad. Sci. U. S. A.* **2014**, *111*, 13481–13486.
65. Fang, R. H.; Hu, C. M.; Chen, K. N.; Luk, B. T.; Carpenter, C. W.; Gao, W.; Li, S.; Zhang, D. E.; Lu, W.; Zhang, L. Lipid-Insertion Enables Targeting Functionalization of Erythrocyte Membrane-Cloaked Nanoparticles. *Nanoscale* **2013**, *5*, 8884–8888.
66. Hu, C. M.; Fang, R. H.; Luk, B. T.; Chen, K. N.; Carpenter, C.; Gao, W.; Zhang, K.; Zhang, L. 'Marker-of-Self' Functionalization of Nanoscale Particles through a Top-Down Cellular Membrane Coating Approach. *Nanoscale* **2013**, *5*, 2664–2668.
67. Jiang, L.; Zhou, Q.; Mu, K.; Xie, H.; Zhu, Y.; Zhu, W.; Zhao, Y.; Xu, H.; Yang, X. Ph/Temperature Sensitive Magnetic Nanogels Conjugated with Cy5.5-Labled Lactoferrin for MR and Fluorescence Imaging of Glioma in Rats. *Biomaterials* **2013**, *34*, 7418–7428.